JB
Journals.ASM.org

Kinetics of *nif* Gene Expression in a Nitrogen-Fixing Bacterium

César Poza-Carrión, Emilio Jiménez-Vicente, Mónica Navarro-Rodríguez, Carlos Echavarri-Erasun, Luis M. Rubio

Centro de Biotecnología y Genómica de Plantas, Universidad Politécnica de Madrid, Madrid, Spain

Nitrogen fixation is a tightly regulated trait. Switching from N_2 fixation-repressing conditions to the N_2-fixing state is carefully controlled in diazotrophic bacteria mainly because of the high energy demand that it imposes. By using quantitative real-time PCR and quantitative immunoblotting, we show here how nitrogen fixation (*nif*) gene expression develops in *Azotobacter vinelandii* upon derepression. Transient expression of the transcriptional activator-encoding gene, *nifA*, was followed by subsequent, longer-duration waves of expression of the nitrogenase biosynthetic and structural genes. Importantly, expression timing, expression levels, and NifA dependence varied greatly among the *nif* operons. Moreover, the exact concentrations of Nif proteins and their changes over time were determined for the first time. Nif protein concentrations were exquisitely balanced, with FeMo cofactor biosynthetic proteins accumulating at levels 50- to 100-fold lower than those of the structural proteins. Mutants lacking nitrogenase structural genes or impaired in FeMo cofactor biosynthesis showed overenhanced responses to derepression that were proportional to the degree of nitrogenase activity impairment, consistent with the existence of at least two negative-feedback regulatory mechanisms. The first such mechanism responded to the levels of fixed nitrogen, whereas the second mechanism appeared to respond to the levels of the mature NifDK component. Altogether, these findings provide a framework to engineer N_2 fixation in nondiazotrophs.

The Mo nitrogenase is responsible for most biological nitrogen fixation (BNF) activity in the biosphere, and due to its great agronomic importance, it has been the subject of thorough genetic and biochemical studies. Although BNF is carried out by only a few species of bacteria and archaea denominated as diazotrophs, there is much interest in the possibility of engineering N_2 fixation activity into nondiazotrophic organisms, including crop plants (1).

The Mo nitrogenase is composed of two oxygen-sensitive metalloproteins designated NifDK and NifH. The NifDK component is a tetramer of the *nifD* and *nifK* gene products that carries one iron-molybdenum cofactor (FeMo-co [7Fe-9S-Mo-C-homocitrate]) buried in the active site of each NifD subunit and one P cluster ([8Fe-7S] cluster) at each NifD-NifK dimer interface (2). NifH is a dimer of the *nifH* gene product that carries one [4Fe-4S] cluster at the subunit interface and serves as an obligate electron donor to the NifDK component (3).

A number of nitrogen fixation (*nif*) gene products work coordinately in the assembly of nitrogenase components in *Azotobacter vinelandii* and other diazotrophs. NifH biogenesis solely requires the activities of the NifU/NifS machinery to provide its [4Fe-4S] cluster (4) and NifM (5). In contrast, many Nif proteins, including NifH, are involved in NifDK biogenesis, mainly due to the structural complexity of FeMo-co (Fig. 1). NifU and NifS provide NifB with [Fe-S] cluster substrates to generate the NifB cofactor (NifB-co), a biosynthetic intermediate, not only for FeMo-co but also for the analogous FeV cofactor (FeV-co) and FeFe cofactor (FeFe-co) of the V and Fe nitrogenases, respectively (6–8). NifB-co is then transferred to NifEN, where additional Fe, Mo, and homocitrate are subsequently incorporated into the cofactor with the aid of NifQ, NifH, and NifV activities (9, 10). Completed FeMo-co is finally incorporated into a FeMo-co-deficient apo-NifDK via NafY to yield the holo-NifDK protein (11). Importantly, NafY has a second role as a chaperone that stabilizes FeMo-co-deficient apo-NifDK in preparation for FeMo-co insertion (12).

Nitrogenase biosynthesis and N_2 fixation activity are energy-demanding processes (13). Thus, *nif* gene expression is tightly controlled by the bacterium. The NifA activator is an enhancer-binding protein that binds to specific DNA sequences upstream of *nif* genes (upstream activator sequences [UASs]) and interacts with the σ^{54} subunit of the RNA polymerase to initiate transcription (14, 15). NifA is active under nitrogen-limiting conditions. The NifL antiactivator is a flavoprotein that senses cellular redox status and binds NifA to block its activity when conditions are not optimal for N_2 fixation. Conditions of nitrogen excess also lead to inactive NifA protein through the formation of a GlnK/NifL/NifA complex. This regulatory mechanism also applies to changes in nitrogen status derived from endogenously fixed nitrogen. Thus, expression of the NifA regulon should respond to the level of nitrogenase activity, and Nif-minus mutants are likely to lack appropriate feedback regulatory mechanisms.

The *nif* regulon is defined as *nifA* and those genes under the control of NifA that are responsible for the production of a functional Mo nitrogenase. In *A. vinelandii*, *nif* genes are clustered in two chromosomal regions comprising at least eight operons (7, 16–18). The major *nif* cluster contains the *nifHDKTYENX*, *iscA*^{nif}, *nifUSV*, *cysE1*^{nif}, *nifWZM*, *clpX2*, and *nifF* genes and other interspersed open reading frames. The minor *nif* cluster contains the *nifLAB*, *fdxN*, *nifOQ*, *rhdN*, and *grx5*^{nif} genes in one transcrip-

Received 14 August 2013 **Accepted** 11 November 2013
Published ahead of print 15 November 2013
Address correspondence to Luis M. Rubio, lm.rubio@upm.es.
C.P.-C. and E.J.-V. contributed equally to this article.
Supplemental material for this article may be found at http://dx.doi.org/10.1128/JB.00942-13.
Copyright © 2014, American Society for Microbiology. All Rights Reserved.
doi:10.1128/JB.00942-13

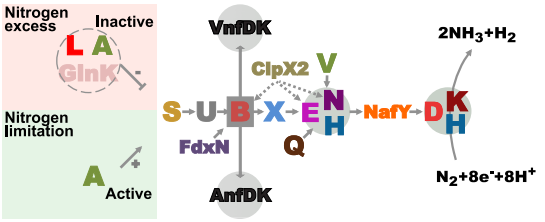

FIG 1 Schematic model of proteins involved in the formation of active nitrogenases in *A. vinelandii*. Nif proteins are indicated by using the last letter of their names. Gray circles, protein complexes containing NifB-co-derived cofactors (FeMo-co, FeV-co, and FeFe-co); dotted lines, regulation by proteolytic degradation. The function of Nif proteins has been reviewed elsewhere (9, 10).

tional direction and a divergent *rnfABCDGEH* and *nafY* gene cluster.

A genome-wide transcription profile analysis comparing steady-state gene expression levels in N_2-fixing *A. vinelandii* cells versus NH_4^+-assimilating cells has recently been carried out and revealed that 400 genes are differentially expressed under Mo-dependent diazotrophic growth conditions (19). A synthetic biology approach to reorganize and simplify the regulation of *nif* genes in *Klebsiella pneumoniae* has recently been reported (20). With the goal of providing a framework to engineer N_2 fixation in nondiazotrophs, we have investigated the time course of expression of nitrogenase components in *A. vinelandii* cells initiating diazotrophic growth, including the exact concentrations of Nif proteins and their variations over time.

MATERIALS AND METHODS

***A. vinelandii* strains and growth conditions.** Strains UW140 (Δ*nifB*) (21), DJ33 (Δ*nifDK*) (22), and UW356 (Δ*nifA*::spc) (23) have been previously described. Strain UW344, bearing an in-frame deletion of *fdxN* (Δ*fdxN*), was generated as described in the supplemental material.

A. vinelandii strains were cultivated in Burk's modified medium (24) at 30°C with or without nitrogen sources, as indicated. Antibiotics were added at standard concentrations (23).

For nitrogenase derepression experiments (diazotrophic growth conditions), NH_4^+-grown cells were diluted in fresh NH_4^+-containing medium at an optical density at 600 nm (OD_{600}) of 0.005 and further cultivated for 17 h. Cells were then collected by centrifugation, washed with NH_4^+-free or NH_4^+-containing medium (control cultures), and resuspended in the same medium at a final OD_{600} of 0.5. Cells were then incubated at 30°C with shaking (200 rpm) in independent Erlenmeyer flasks. At different times, samples were collected and subjected to the following analyses: determination of *in vivo* acetylene reduction activity, cell volume determination, OD_{600} determination, quantitative real-time PCR (qRT-PCR), and quantitative immunoblotting.

Plasmid constructions and DNA manipulations. Plasmid constructions, PCR, and transformation of *Escherichia coli* were carried out by standard methods (25). *E. coli* strains were cultivated in Luria-Bertani medium at 37°C with shaking (200 rpm). Antibiotics were added at standard concentrations (25).

Plasmid pRHB470 carries a synthetic DNA fragment containing the amplicons from the *nifH*, *nifD*, *nifK*, *nifY*, *nifE*, *nifN*, *nifX*, *nifU*, *nifS*, *nifV*, *nifA*, *nifB*, *fdxN*, *nifQ*, and *nafY* genes, tested in qRT-PCRs, cloned into the NotI site of pUC57. Plasmid pRHB506 carries a synthetic DNA fragment containing the amplicons from 16S rRNA and *nifL* genes cloned into the NotI site of pUC57. Plasmids pRHB470 and pRHB506, used as standards in qRT-PCRs, were generated by Proteogenix and GenScript, respectively.

To generate the Δ*fdxN* mutant, an in-frame *fdxN* deletion was introduced into the *A. vinelandii* chromosome. Flanking regions of the *fdxN* gene were generated by PCR using the oligonucleotides 5′-GCGGAATTCGCCTGATCAACCAGCACTTC-3′ and 5′-CCAGGATCCACCTCCACGCAATCCTCGAAT-3′ for the *nifB* region upstream of *fdxN* and 5′-CCCGGATCCGAGAGTCGCCATGACCAGCA-3′ and 5′-CTCGAATTCGAGGTGGTTGGCTCTGTCAT-3′ for the *nifO* region downstream of *fdxN*. The EcoRI (GAATTC) and BamHI (GGATCC) restriction sites incorporated into the oligonucleotides to facilitate vector construction are shown underlined in the oligonucleotide sequences. The resulting products were digested with EcoRI-BamHI and cloned into pGEM11Zf(+) (Promega) either by triple ligation reactions to generate plasmid pRHB312 or by quadruple ligations together with a BamHI-digested kanamycin resistance cassette to generate pRHB308.

The procedures used for *A. vinelandii* transformation and gene replacement have been described previously (26). Plasmid pRHB308 was introduced into the chromosome of the *A. vinelandii* DJ strain by homologous recombination to generate strain UW353. Strain UW344, bearing an in-frame Δ*fdxN* mutation, was isolated by cotransforming (congression) strain UW353 with plasmids pRHB312 and pDB303, which contains a rifampin resistance marker (kindly provided by D. Dean). Preliminary identification of Δ*fdxN* mutants was verified on rifampin-containing solid medium by the phenotypic loss of kanamycin resistance, which was further confirmed by PCR analysis and sequencing of the locus using genomic DNA of the mutant strains. Isolation of genomic DNA from *A. vinelandii* strains was performed with a DNeasy tissue kit (Qiagen).

All DNA constructions were confirmed by restriction analysis and by DNA sequencing. The *A. vinelandii* strains generated were confirmed by PCR analysis and, when possible, by immunoblot analysis with appropriate antibodies.

RNA isolation and absolute qRT-PCR analyses. The *A. vinelandii* DJ (wild type), Δ*fdxN*, Δ*nifA*, Δ*nifB*, and Δ*nifDK* strains were grown as described above. Each biological replicate for qRT-PCR experiments consisted of a 20-ml cell culture harvested by centrifugation at 5,000 × *g* for 5 min at 4°C, quickly frozen in liquid N_2, and stored at −80°C. Total RNA was isolated using a RiboPure-Bacteria kit (Ambion, Life Technologies) according to the manufacturer's instructions. Genomic DNA traces were digested using the Turbo DNA-free reagent (Ambion, Life Technologies). cDNA synthesis was carried out using a High Capacity cDNA reverse transcription kit (Ambion, Life Technologies) following the manufacturer's instructions. Each reaction mixture used 2 μg of total RNA. An aliquot of 1 μl of a 1:10 dilution of the cDNA (1:10,000 for the reference 16S rRNA gene) was used as the template for qRT-PCR amplification.

qRT-PCR experiments were performed using Power SYBR green PCR master mix (Ambion, Life Technologies). The final volume of the reaction mixture was 15 μl per well. A standard Applied Biosystems cycle protocol was used. All samples were run in an Eco real-time PCR system (Illumina). Gene-specific primers were designed with the Primer Express (v2.0) program (Ambion, Life Technologies). Primers with annealing temperatures of between 58°C and 62°C, which amplified products with lengths of ca. 100 bp, were selected and tested for specificity using the BLAST program. The gene-specific primers used for qRT-PCR are listed in Table S1 in the supplemental material. Data acquisition was performed using Eco real-time PCR system software (v4.1; Illumina). At least three independent biological replicates were used for each experiment.

In order to design DNA standards for absolute quantification calculations (27), the efficiency of amplification for each gene was determined using as the template cDNA from *A. vinelandii* DJ grown for 1 h under diazotrophic conditions. Only primers with optimal efficiency were used to design synthetic DNA standards. Plasmids pRHB470 and pRHB506, carrying DNA standards, were linearized using the HindIII restriction enzyme, purified, aliquoted, and stored at 10 pg/μl in diethyl pyrocarbonate-treated H_2O (Ambion, Life Technologies). The dynamic range of the calibration curves was 1,000-fold (10 pg, 5 pg, 1 pg, 0.1 pg, and 0.01 pg).

Sample concentrations were determined by interpolating their quantification cycle (C_q) values into the corresponding standard curve. To compensate for intra- and interkinetic qRT-PCR variations (sample-to-

sample and run-to-run variations), data normalization was performed using the endogenous unregulated gene transcript of 16S rRNA as a reference. The absolute abundance of each gene transcript was divided by the absolute value for 16S rRNA to obtain normalized absolute signal (NAS) values to allow direct comparison of different samples.

DNA motif analysis. Five-hundred-base-pair sequences upstream of the 5′ ATG codon of *A. vinelandii nif* operons were retrieved with the Genome and Gene Information regulatory sequence analysis (RSA) tools to identify specific promoter consensus sequences using pattern-matching tools (one substitution allowed) (http://rsat.ulb.ac.be). Consensus sequences 5′-YTGGCACGR-(N)3-TTGCW for RpoN (28), 5′-WATCAAN NNNTTR for the integration host factor (IHF) (29), and 5′-TGT-$(N)_{10}$-ACA for the NifA-dependent UAS (14) were used to obtain frequency matrices of NifA binding sites upstream of *A. vinelandii nif* promoters. These motifs were assembled into frequency matrices using the pattern assembly tool with default parameters. Matrices were converted into consensus motifs using the convert matrix tool and were displayed using the WebLogo program (30). Positional weight matrices were used to determine the positions and numbers of NifA DNA binding sites in *A. vinelandii* by using matrix-scan RSA tools.

Controls were set with 10 *in silico* experiments in which 100 random sequences of 500 bp in length from the *A. vinelandii* genome were retrieved with build control RSA tools (http://rsat.ulb.ac.be) and analyzed using matrix-scan RSA tools.

Protein methods. The protein concentration was determined by the bicinchoninic acid method with bovine serum albumin as the standard (31). Procedures for SDS-PAGE (32) and immunoblot analysis (33) have been described previously. Protein samples for immunoblot analyses were prepared by mixing pelleted cells with Tris-HCl (100 mM) at a final OD_{600} of 2 and then diluting the samples with 2× Laemmli sample buffer supplemented with 0.1 M dithiothreitol. Fifteen microliters of this mix was loaded per line. Absolute quantification of each protein was performed using a calibration curve obtained with known amounts of the same protein in a purified state. ImageJ software was used to quantify the protein levels in immunoblot membranes.

Purification of the NifB, NifEN, NifH, NifDK, and NifQ proteins from *nif*-derepressed *A. vinelandii* cells was performed under anaerobic conditions. NifB was purified from UW232 cells (21), NifEN was purified from UW243 cells (34), NifH and NifDK were purified from DJ cells (35), and NifQ was purified from UW300 cells (36). NifU was purified under anaerobic conditions from BL21 Rosetta(pRHB252) cells. NifX and NafY and were purified under aerobic conditions from BL21(pREP-4)(pRHB155) cells (34) and from BL21(pREP-4)(pRHB62) cells (11), respectively.

Nitrogenase activity. *In vivo* nitrogenase activities were determined by the acetylene reduction assay at 30°C for 15 min using 1 ml of culture samples, as described previously (37).

Cell volume measurements. *A. vinelandii* cell number and volume were measured with a ZM Coulter Counter with a 30-μm-diameter orifice connected to a C1000 Channelyzer apparatus (Coulter Electronics) after fixing the cells in 0.75% formaldehyde. For each sample, the median of the cell volume and cell number distribution was recorded. One hundred cells were analyzed for each time point.

RESULTS

Time course of *nif* gene expression upon nitrogen step-down. The absolute levels of accumulation of *nif*-specific mRNAs were estimated by quantitative real-time PCR (qRT-PCR) by comparison with the results obtained with known amounts of synthetic DNA amplicons. mRNA levels were then compared to the 16S rRNA level present in each sample to yield normalized absolute signals (NASs). Figure 2 and Fig. S1 in the supplemental material show that *A. vinelandii* responded rapidly to nitrogen step-down by expressing *nif* genes and developing nitrogenase activity. The *nifLA* operon responded fast to nitrogen step-down, with *nifA* exhibiting a narrow wave of expression that peaked 30 min after

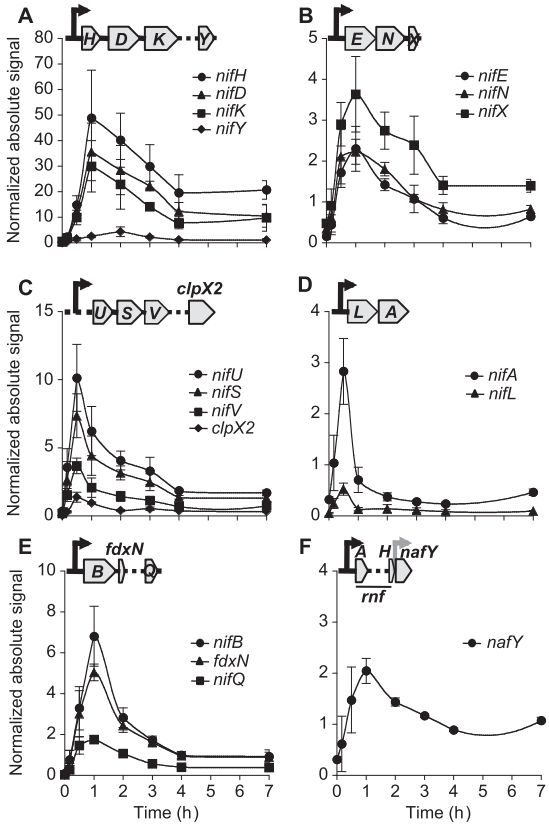

FIG 2 Time-dependent profile of induction of *nif* genes necessary for Mo nitrogenase in *A. vinelandii*. (A to C) Expression levels of genes within the major *nif* cluster, which contains *nifHDKTYENX-iscA*^{nif}*-nifUSV-cysE1*^{nif}*-nifWZM-clpX2-nifF*; (D to F) expression levels of genes within the minor *nif* cluster, which contains *rnfABCDGEH-nafY* in one DNA orientation and *nifLAB-fdxN-nifOQ-rhdN-grx5*^{nif} in the opposite DNA orientation. In all cases, absolute expression levels were estimated by comparison to the levels on standard curves obtained with known amounts of synthetic DNA amplicons and were then normalized to 16S rRNA levels. Black arrows, predicted σ^{54}-dependent promoter regions; gray arrow, a hypothetical constitutive promoter region; dotted lines, unstudied interspersed genes within each operon that have been omitted for clarity. Data are the averages of at least three biological replicates ± SEs.

NH_4^+ removal from the medium (Fig. 2D). Expression of genes within the *iscA*^{nif}*nifUSV-cysE1*^{nif}*-nifWZM-clpX2* cluster also peaked after 30 min, exhibiting NAS values for *nifU*, *nifS*, *nifV*, and *clpX2* of 10, 7.3, 3.6, and 1.8, respectively (Fig. 2C). Most genes involved in FeMo-co biosynthesis (the *nifENX* and *nifB-fdxN-nifOQ* operons and the *nafY* gene) showed maximum mRNA levels 1 h after derepression with NAS values ranging from 2 to 7 (Fig. 2B, E, and F). Similarly, nitrogenase structural genes showed maximum mRNA levels 1 h after derepression, but NAS values were much higher, ranging from 30 to 50 (Fig. 2A). In contrast, *nifY* showed the slowest response, with an accumulation peak at 2 h and a NAS value of 4.3. Two main patterns of mRNA accumulation occurred when nitrogenase activity was at steady state (4 to 7 h after derepression; see Fig. S1 in the supplemental material): *nifH*, *nifD*, *nifK*, *nifE*, *nifN*, *nifX*, and *nafY* levels were at least 25% of their maximum NAS levels 7 h after derepression, whereas the levels for all other genes returned to the basal NAS levels.

No changes in *nif* mRNA levels were observed in control cul-

tures of *A. vinelandii* growing in the presence of NH_4^+ 4 h after inoculation into fresh medium (see Table S2 in the supplemental material).

Operons belonging to the *nif* regulon can be identified by the presence of NifA-binding motifs or UASs (see Fig. S2 in the supplemental material). A correlation between the number of UASs present in *nif* promoter regions and accumulated mRNA levels was found. For example, the 500-bp upstream region controlling expression of *nifHDKTY* contains 3 UASs, whereas *in silico* control experiments determined a random frequency of 1.26 UASs for a 500-bp DNA region across the *A. vinelandii* genome. This correlation suggests positive cooperativity in NifA binding to UASs or in NifA activation of polymerase.

Time course of Nif protein accumulation upon nitrogen step-down. The intracellular accumulation of a number of Nif proteins was estimated by quantifying the *A. vinelandii* whole-cell immunoblot signals against a standard curve generated by immunoblotting known amounts of the corresponding purified Nif protein (see Fig. S3 in the supplemental material) and dividing by the total cell volume in the sample. Consistent with its role in the general synthesis of [Fe-S] clusters for both nitrogenase structural and biosynthetic proteins, NifU accumulated rapidly, showing 90% of its maximum value of 23.7 μM 1 h after derepression (Fig. 3A). FeMo-co biosynthetic proteins showed relatively low accumulation levels, ranging from 0.4 μM for NifEN to 3.2 μM for NifB, 5.7 μM for NifQ, and 5.8 μM for NifX (Fig. 3B). On the other hand, nitrogenase structural proteins accumulated to very high levels 4 h after derepression: 108.5 μM for NifH, 54.8 μM for NifD, and 48.1 μM for NifK (Fig. 3C). The NafY chaperone that is involved in stabilizing FeMo-co-deficient apo-NifDK showed significant basal levels (8 μM) at the start of derepression, with levels increasing moderately over time (up to 19.9 μM).

At the time of maximum *in vivo* nitrogenase activity (4 h after derepression), the nitrogenase proteins could be grouped into three main categories according to their levels: (i) low-concentration proteins involved in FeMo-co biosynthesis, NifE (0.4 μM), NifN (0.3 μM), NifB (2.7 μM), and NifQ (2.5 μM); (ii) midconcentration proteins dedicated to the transfer or storage of FeMo-co and its precursors, NifX (5.8 μM) and NafY (17.7 μM); and (iii) high-concentration proteins, NifD (54.8 μM), NifK (48.1 μM), and NifH (107.2 μM). Finally, NifU (23.7 μM) did not fit easily into the group of FeMo-co biosynthesis proteins, which is consistent with its role in providing [Fe-S] clusters to many different proteins.

The maximum mRNA concentration/maximum protein concentration ($[mRNA]_{max}/[protein]_{max}$) ratio was used as an index to understand the relationship between mRNA stability and protein accumulation (Table 1). Although this index varied between 0.3 and 0.6 in most cases, a few significant exceptions were found. The *nafY* mRNA/NafY index was 0.10, which suggested either a high degree of stability of the NafY chaperone or highly translated *nafY* mRNA. On the other hand, the *nifN* mRNA/NifN, *nifE* mRNA/NifE, and *nifB* mRNA/NifB indexes were 4.70, 4.16, and 2.12, respectively, consistent with targeted degradation of NifB and NifEN during diazotrophic growth by ClpX2 (38).

Gene expression in the Δ*nifA* mutant. As expected, the Δ*nifA* mutant exhibited a Nif-minus phenotype and lacked *in vivo* nitrogenase activity. *nifH*, *nifD*, *nifK*, and *nifY* mRNA levels in the Δ*nifA* strain were negligible: 390-, 170-, 120-, and 130-fold lower than the level in the wild type, respectively (Fig. 4A). Similarly, the

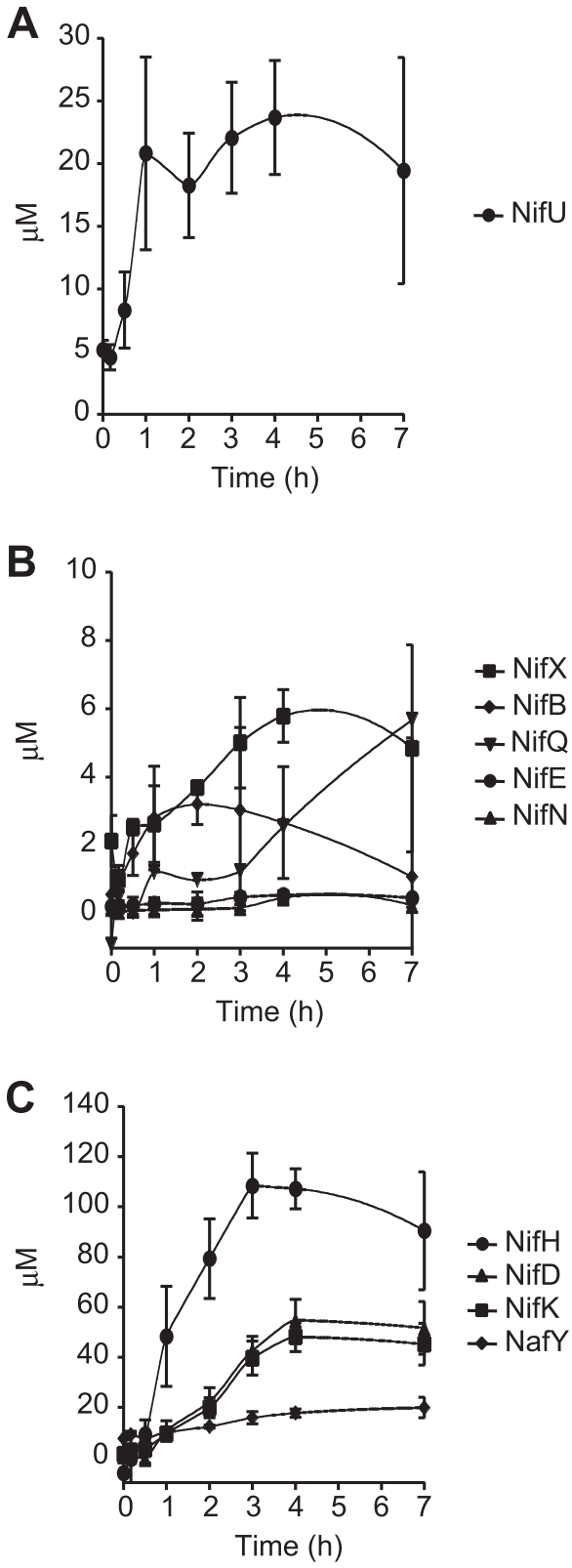

FIG 3 Time course of Nif protein accumulation in *A. vinelandii*. (A) NifU protein, required for the biosynthesis of [Fe-S] clusters for the nitrogenase components; (B) FeMo-co biosynthetic proteins; (C) nitrogenase structural proteins, including the NafY chaperone.

TABLE 1 Comparison of $[mRNA]_{max}/[protein]_{max}$ ratios between the wild-type and Δ*fdxN A. vinelandii* strains

Protein	$[mRNA]_{max}/[protein]_{max}$[a]	
	Wild type	Δ*fdxN* mutant
NifU	0.43	0.46
NifB	2.12	1.03
NifX	0.63	1.44
NifE	4.16	2.20
NifN	4.70	3.44
NifQ	0.31	0.11
NafY	0.10	0.08
NifD	0.65	1.58
NifK	0.62	1.36
NifH	0.45	0.62

[a] Maximum levels of mRNA (NASs) and protein (μM) were used to calculate these ratios.

nifENX and *nifB-fdxN-nifOQ* operons showed large drops in expression compared to the levels in the wild type: 43-fold lower levels of mRNA for *nifE*, 75-fold lower levels for *nifN*, 20-fold lower levels for *nifX*, 270-fold lower levels for *nifB*, 44-fold lower levels for *fdxN*, and 17-fold lower levels for *nifQ*. Genes within the *iscA*^{nif}*-nifUSV-cysE1*^{nif}*-nifWZM-clpX2* cluster were not as drastically dependent on NifA, since *nifU*, *nifS*, *nifV*, and *clpX2* mRNA levels were 3, 4, 9, and 4 times lower than those in the in wild type, respectively. However, their time course expression profiles showed some response to nitrogen step-down, exhibiting mRNA induction ratios of 152, 66, 29, and 19 for *nifU*, *nifS*, *nifV*, and *clpX2*, respectively (see Fig. S4 in the supplemental material). Finally, *nafY* mRNA levels were reduced 10-fold with respect to the level for the wild type, a value lower than that previously reported (12).

Deletion of the *fdxN* gene alters *nif* gene expression and Nif protein accumulation. The *fdxN* gene, located between *nifB* and *nifQ* in the minor *nif* cluster, encodes a ferredoxin with similarity to 2×[4Fe-4S]. Deletion of *fdxN* resulted in a 4-fold decrease in NifDK activity. The Δ*fdxN* strain consistently accumulated higher levels of *nif*-specific transcripts than the wild type, except for lower *nifY* and *nifQ* mRNA levels and the absence of *fdxN* expression (Fig. 4B). Seven hours after derepression, all genes tested presented higher mRNA levels in the Δ*fdxN* mutant than in the wild type (see Fig. S5 in the supplemental material).

Other fundamental differences in *nif* expression profiles were observed between the Δ*fdxN* and the wild-type strains. First, *nifA* and *nifL* mRNA levels did not decrease rapidly, as in the wild type, but, rather, stayed at maximum levels for 2 to 3 h after derepression (see Fig. S5 in the supplemental material). Second, the response to nitrogen step-down was generally delayed, with most mRNAs showing maximum accumulation levels 2 to 3 h after derepression and with the levels descending slowly over the 7-h period studied here (Fig. 4B).

The time course of Nif protein accumulation in the Δ*fdxN* mutant was different from that in the wild type (Fig. 5). The maximum concentration of NifH was 1.4-fold higher in the Δ*fdxN*

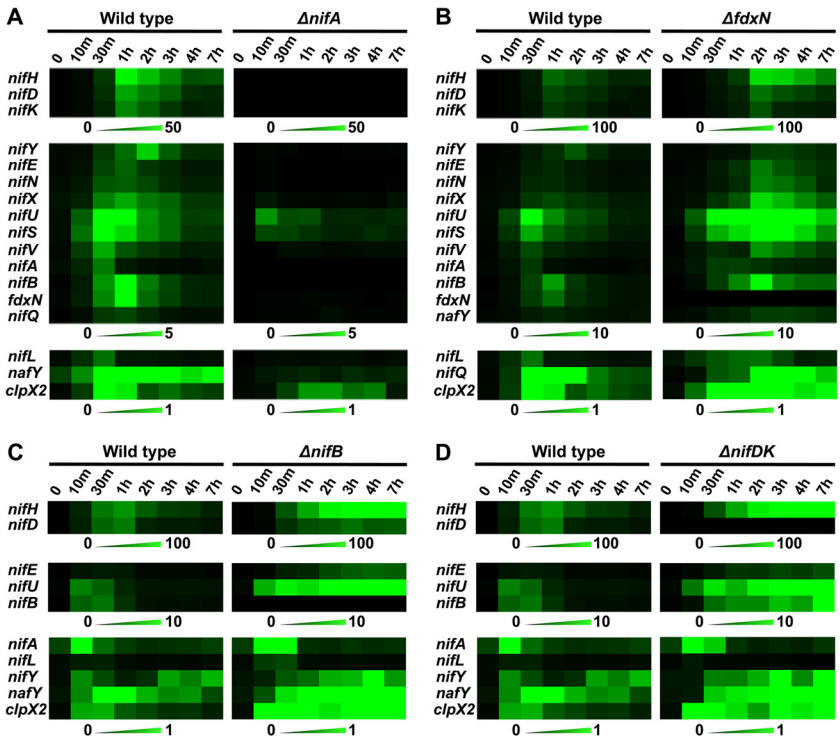

FIG 4 Different responses to the change toward diazotrophic growing conditions in *A. vinelandii*. (A) Wild type versus the Δ*nifA* mutant, which lacks the transcriptional activator NifA; (B) wild type versus the Δ*fdxN* mutant, which is partially impaired in FeMo-co biosynthesis; (C) wild type versus the Δ*nifB* mutant, which is completely impaired in FeMo-co biosynthesis; (D) wild type versus the Δ*nifDK* mutant, which lacks the nitrogenase structural genes NifDK. mRNA expression data were visualized with the MultiExperiment Viewer program (http://www.tm4.org/). The scale color bars show mRNA-normalized absolute signals: black, a lack of mRNA; bright green, the maximum mRNA level in each experiment. Each data point represents the mean of at least three biological replicates.

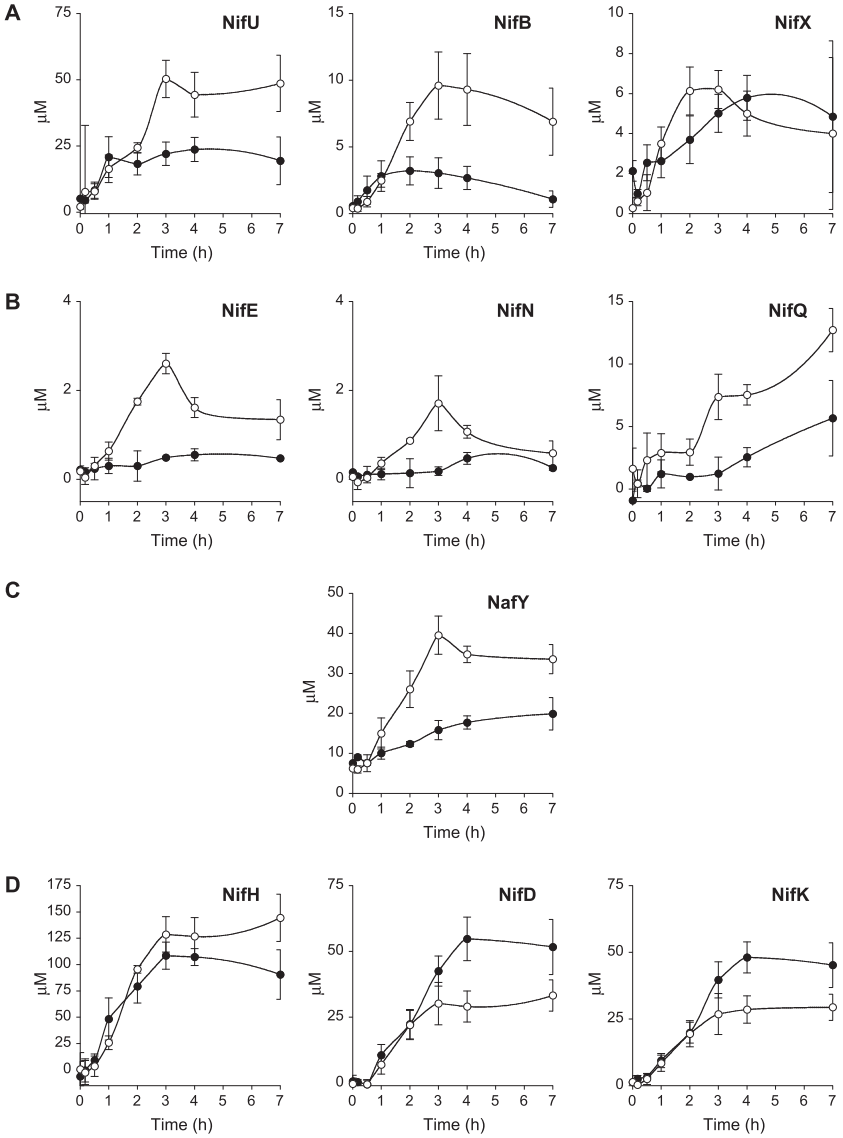

FIG 5 Time-dependent profile of Nif protein accumulation upon nitrogen step-down in wild-type *A. vinelandii* (closed symbols) and the Δ*fdxN* mutant (open symbols). Proteins are organized by their role in nitrogenase biogenesis: proteins involved in early steps of FeMo-co synthesis (A), proteins involved in late steps of FeMo-co synthesis (B), proteins involved in FeMo-co insertion into apo-NifDK (C), and nitrogenase structural proteins (D). The total cell volume was used to calculate protein concentrations (μM). Data are the averages of three biological replicates ± SEs.

mutant (144.5 μM) than in the wild type (107.2 μM). In contrast, NifD and NifK followed the opposite trend, with maximum concentrations being almost 2-fold lower in the mutant than in the wild type (33.2 μM and 29.4 μM, respectively). Importantly, the Δ*fdxN* strain accumulated as much NafY chaperone as NifD and NifK, suggesting the need to stabilize apo-NifDK, probably because of a defect in FeMo-co biosynthesis. Δ*fdxN* also accumulated higher concentrations of NifU (2.6-fold) and the FeMo-co biosynthetic proteins NifB (3.1-fold), NifEN (5.3-fold), and NifQ (2.3-fold) than the wild type. The levels of NifX, which has been proposed to function as a reservoir for FeMo-co precursors (34), were similar in the wild-type and Δ*fdxN* strains.

***nif* gene expression in Δ*nifB* and Δ*nifDK* mutants.** The marked effect of the Δ*fdxN* mutation on *nif* gene expression prompted us to investigate the response of *A. vinelandii* to nitrogen step-down in mutants unable to fix N_2. Two different Nif-minus strains were selected: a Δ*nifB* mutant that was impaired at the early steps of FeMo-co biosynthesis and thus unable to accumulate cofactor biosynthetic intermediates and a Δ*nifDK* mutant that had no defect on FeMo-co biosynthesis but was unable to fix N_2.

The Δ*nifB* and Δ*nifDK* mutants exhibited *nifA* and *nifL* mRNA levels (see Fig. S6 and S7 in the supplemental material) and expression profiles (Fig. 4C and D) similar to those in the wild type. However, this was not the case for the other *nif* genes, where mRNAs were observed to accumulate at very high levels in the mutants (Fig. 4C and D). Seven hours after switching to diazotrophic growth conditions, the Δ*nifDK* mutant accumulated 9-fold more *nifH* mRNA than the wild type (see Fig. S6 in the supplemental material), whereas the Δ*nifB* strain accumulated 10-

fold more *nifH* mRNA and 4-fold more *nifD* mRNA than the wild type (see Fig. S7 in the supplemental material). The *nifB*, *nifE*, *nifU*, and *nafY* genes, whose products are involved in biosynthesis and insertion of FeMo-co, were also more highly expressed in both mutants (except for the lack of *nifB* mRNA in the Δ*nifB* mutant). Interestingly, *clpX2* showed unusual peaks of expression over time, with a maximum 18-fold higher level of expression in the Δ*nifB* mutant and an 8-fold higher level of expression in the Δ*nifDK* mutant than in the wild type.

DISCUSSION

A. vinelandii responds in a highly coordinated manner to nitrogen step-down in preparation for diazotrophic growth. Expression from the *nifLA* operon, encoding the regulatory proteins NifL and NifA, was observed early after nitrogen step-down (14, 15). Maximum *nifA* mRNA accumulation occurred 10 to 30 min after NH_4^+ removal from the medium. However, at 1 h after derepression, *nifA* mRNA levels were barely detectable (Fig. 2). Expression of *nifL* followed an identical pattern, but *nifL* mRNA levels were considerably lower, even though *nifL* is located closer to the promoter of the *nifLA* operon. Since there are no apparent additional promoters upstream of *nifA*, a plausible scenario could be that *nifL* has a higher rate of mRNA degradation than *nifA*. A possible mechanism for this could be through specific noncoding RNAs that are capable of targeting *nifL* mRNA for degradation, such as the one described previously (39). The DNA region upstream of *nifLA* contains one RpoN (σ^{54})-binding motif and two NifA-binding UASs, suggesting that NifA autoregulates expression of the *nifLA* operon. Consistent with this, very low *nifL* mRNA levels were observed in the Δ*nifA* mutant.

Rapid accumulation of the *nifU*, *nifS*, *nifV*, and *clpX2* mRNAs was also observed, but their pattern of disappearance was not as drastic as that for *nifL* and *nifA* (Fig. 2). The products of *nifU* and *nifS* are involved in [Fe-S] cluster biosynthesis for both nitrogenase components (18), including providing precursors for the early stages of FeMo-co biosynthesis (6). The product of *clpX2* is part of a protease system that specifically targets the NifB and NifEN proteins for degradation (38). Expression of the *nifU*, *nifS*, and *nifV* genes, whose products are required for all three nitrogenases in *A. vinelandii* (40), was not completely eliminated in the Δ*nifA* mutant. One RpoN-binding motif and two putative AnfA-binding sites are located upstream of $iscA^{nif}$ and also between $iscA^{nif}$ and *nifU*, suggesting that expression of the $iscA^{nif}$-*nifUSV*-$cysE1^{nif}$-*nifWZM*-*clpX2* operon is also under the control of AnfA. It has previously been shown that an *A. vinelandii nifA* mutant was able to express V or Fe nitrogenases when molybdate was not present in the growth medium (40) and that the VnfA and AnfA transcriptional activators (which regulate the expression of the *vnf* and *anf* genes of the V- and Fe-only nitrogenases, respectively) were able to modulate the expression of *nifB* (41) and *nifM* (42). However, it should be noted that both VnfA and AnfA are poorly expressed when molybdate is present in the growth medium (43).

This study provides accurate quantification of expression strength in terms of mRNA and Nif protein accumulation as well as the timing of expression required for N_2 fixation. The expression of most of the genes studied here peaked 1 to 2 h after derepression. Importantly, expression of the *nifB*-*fdxN*-*nifOQ*-*rhdN*-$grx5^{nif}$ operon appears to end earlier than that of the *nifHDKTY* operon (Fig. 2), suggesting a correlation between expression timing and protein function. We found that, in general, genes required for the early stages of nitrogenase biosynthesis, i.e., *nifU*, *nifS*, *fdxN*, and *nifB*, were expressed and turned off earlier than genes required in later stages of the pathway. Our results suggest that proper expression dynamics could be important in the context of engineering nitrogen fixation in nondiazotrophs. The incorporation of genetic circuits adding temporal control to *nif* gene expression must be considered by the synthetic biologist. Recently, the *K. pneumoniae nif* gene cluster has been refactored by using synthetic biology tools that removed all native regulation (20). The resulting refactored strain showed 7% of wild-type nitrogenase activity and 3.5-fold lower diazotrophic growth rate. We argue that controlling the timing of metalloprotein maturation in this biosynthetic pathway could result in increased activities. For instance, initial synthesis of [Fe-S] clusters by NifS and NifU might be important to properly fold metalloproteins, such as NifEN or NifDK.

Although each *nif* operon yielded similar mRNA levels for the genes that it contains, clear exceptions were found in the cases of *nifL* (described above), *nifY*, and *nifQ*. The *nifY* mRNA levels were 10-fold lower than those of *nifH*, *nifD*, and *nifK*, while *nifQ* had 4-fold lower mRNA levels than *nifB* and *fdxN*. The presence of intergenic secondary structures within the *nifHDKTY* operon that affect mRNA levels has been described (19). Likewise, the lower level of expression of *nifQ* with respect to that of *nifB* and *fdxN* has been reported previously (44). We hypothesize that mRNA stability within *nif* operons may be modulated by the presence of uncharacterized noncoding RNAs.

The accumulation pattern of Nif proteins indicates that the diazotrophic cell is capable of maximizing its resources by logically arranging protein synthesis on the basis of protein functions. NifU was the first protein to reach maximum accumulation (Fig. 3), in accordance with its foundational role in [Fe-S] cluster biosynthesis for nitrogenase components, including the early steps in FeMo-co biosynthesis. However, NifH was the most prevalent protein 1 h after derepression and remained so during the next 6 h. It is possible that early NifH abundance is required to support P-cluster (45) and FeMo-co (46) syntheses. NifH achieved its maximum concentration 4 h after derepression, coinciding with the maximum NifDK concentration and the maximum *in vivo* nitrogenase activity. This was in line with the structural role of NifH in the nitrogenase complex. The observed *in vivo* NifH/NifDK molar ratio was 2 at the time when maximum nitrogenase activity occurred. This is in contrast to the optimum ratio in the *in vitro* assays, which was reported to be 40 NifH to 1 NifDK (47).

Once nitrogenase was fully operational, the demand for biosynthetic components, such as NifB and NifEN, decreased. NifB catalyzes the biosynthesis of NifB-co, an early intermediate in the FeMo-co biosynthetic pathway (8). Similar to NifU, the NifB concentration was the highest 1 h after derepression (3 μM), but it was observed to slowly decrease to 1 μM after 7 h of derepression. NifE and NifN polypeptide concentrations were similar throughout the experiment, consistent with the stoichiometric requirement to form the $NifE_2$-$NifN_2$ heterotetramer in which FeMo-co is assembled (9). The NifEN/NifDK molar ratio also decreased over time from 0.02 at 1 h after derepression to 0.007 after 7 h. The fact that NifB and NifEN are actively degraded during diazotrophic growth (38) may explain their very low concentrations. However, it is likely that NifB and NifEN are able to perform multiple enzymatic turnovers *in vivo* in order to provide sufficient FeMo-co for an excess of NifDK molecules.

In contrast to other biosynthetic proteins, the concentrations of NifQ and NafY steadily increased, suggesting that they are needed during and after the initial diazotrophic growth stages (Fig. 3). The roles of NafY in apo-NifDK stabilization and in FeMo-co insertion to form holo-NifDK (48) might be still required at later stages. The NifQ accumulation pattern is difficult to interpret, as its role is to donate the Mo atom to the NifEN/NifH complex for its incorporation into FeMo-co (36), and therefore, a pattern of accumulation similar to that of NifB or NifEN was expected.

New insights into the timing and regulation of *nif* expression were obtained from the study of the Δ*fdxN* mutant. The Δ*fdxN* strain has been suggested to be partially impaired in FeMo-co biosynthesis (44). The pattern of *nif* gene expression in this mutant was characterized by a lag in the expression of *nif* genes and increased *nif* mRNA accumulation (see Fig. S5 in the supplemental material). This delay may reflect the need to recycle proteins due to a low nitrogen-fixing activity. Importantly, *nifL* and *nifA* mRNA levels were increased, which might result in increased levels of NifA activity and, in turn, elevated levels of *nif* transcripts and of accumulated Nif proteins (with the exception of the NifDK protein, as discussed below). It is important to note that the increase of *nifLA* mRNA levels is not a general effect of mutants impaired in nitrogenase activity because the Δ*nifB* and Δ*nifDK* mutants showed wild-type profiles of *nifLA* expression. Thus, it is possible that FdxN has an additional regulatory role besides its role in FeMo-co biosynthesis.

Although *nifD* and *nifK* mRNA levels remained high during derepression in the Δ*fdxN* strain, the NifDK protein was much less abundant, and therefore, the corresponding $[\text{mRNA}]_{\text{max}}/[\text{protein}]_{\text{max}}$ index was significantly higher than that in the wild type. In addition, NafY was more abundant in the Δ*fdxN* mutant, reaching an equimolecular concentration with NifDK. It is known that apo-NifDK is less stable than holo-NifDK and that NafY associates with and stabilizes the FeMo-co-deficient apo-NifDK (11, 48). Altogether, these observations suggest that the Δ*fdxN* mutant accumulates significant amounts of FeMo-co-deficient apo-NifDK. It also accumulated 3-fold the amount of FeMo-co biosynthetic proteins, including NifU, NifS, NifB, NifE, NifN, and NifQ, compared to wild type (the NifH concentration increased 1.4-fold), probably to compensate for its impairment in FeMo-co biosynthesis. The stoichiometries among the biosynthetic proteins remained almost identical, as if the fine-tuned regulation coordinating FeMo-co biosynthesis was not affected.

Finally, the Δ*nifB* and Δ*nifDK* mutants, which are unable to fix N_2 and therefore remain under nitrogen starvation, responded to derepression by accumulating very high levels of *nif* mRNAs. It has previously been observed that cultures derepressed under argon showed exacerbated nitrogenase activity levels in a phenomenon termed hyperderepression (49). The mechanism by which *A. vinelandii* detects a defect in nitrogenase biosynthesis or activity and then overcompensates for this defect is not well understood, but it is possible that NifL could be less inhibitory in these situations, leading to increased NifA activity. This effect is consistent with the nitrogen feedback regulatory response mediated by NifL. Indeed, fixed nitrogen exerts negative feedback regulation over *nif* gene expression. In the wild-type strain, the initial burst of *nif* gene expression followed by a reduction toward steady-state levels is reminiscent of the behavior of other negative-feedback-regulated systems, such as the ornithine transcarbamylase activity in the arginine biosynthetic pathway of *E. coli* (50). Interestingly, *nifA* and *nifL* mRNA accumulation was unaltered in the Δ*nifB* and Δ*nifDK* mutants, suggesting that the inability to synthesize mature NifDK itself affects NifA activity by a mechanism different from (or in addition to) that involving the level of fixed nitrogen.

ACKNOWLEDGMENTS

This work was supported by ERC starting grant 205442 (to L.M.R.) and MICINN grant BIO2009-12661 (to L.M.R.)

We thank Ryan Kniewel for critically reading the manuscript.

REFERENCES

1. **Beatty PH, Good AG.** 2011. Future prospects for cereals that fix nitrogen. Science **333:**416–417. http://dx.doi.org/10.1126/science.1209467.
2. **Spatzal T, Aksoyoglu M, Zhang L, Andrade SL, Schleicher E, Weber S, Rees DC, Einsle O.** 2011. Evidence for interstitial carbon in nitrogenase FeMo cofactor. Science **334:**940. http://dx.doi.org/10.1126/science.1214025.
3. **Georgiadis MM, Komiya H, Chakrabarti P, Woo D, Kornuc JJ, Rees DC.** 1992. Crystallographic structure of the nitrogenase iron protein from *Azotobacter vinelandii*. Science **257:**1653–1659. http://dx.doi.org/10.1126/science.1529353.
4. **Dos Santos PC, Smith AD, Frazzon J, Cash VL, Johnson MK, Dean DR.** 2004. Iron-sulfur cluster assembly: NifU-directed activation of the nitrogenase Fe protein. J. Biol. Chem. **279:**19705–19711. http://dx.doi.org/10.1074/jbc.M400278200.
5. **Howard KS, McLean PA, Hansen FB, Lemley PV, Koblan KS, Orme-Johnson WH.** 1986. The *Klebsiella pneumoniae nifM* gene product is required for stabilization and activation of nitrogenase iron protein in *Escherichia coli*. J. Biol. Chem. **261:**772–778.
6. **Zhao D, Curatti L, Rubio LM.** 2007. Evidence for *nifU* and *nifS* participation in the biosynthesis of the iron-molybdenum cofactor of nitrogenase. J. Biol. Chem. **282:**37016–37025. http://dx.doi.org/10.1074/jbc.M708097200.
7. **Joerger RD, Bishop PE.** 1988. Nucleotide sequence and genetic analysis of the *nifB-nifQ* region from *Azotobacter vinelandii*. J. Bacteriol. **170:**1475–1487.
8. **Shah VK, Allen JR, Spangler NJ, Ludden PW.** 1994. In vitro synthesis of the iron-molybdenum cofactor of nitrogenase. Purification and characterization of NifB cofactor, the product of NifB protein. J. Biol. Chem. **269:**1154–1158.
9. **Rubio LM, Ludden PW.** 2008. Biosynthesis of the iron-molybdenum cofactor of nitrogenase. Annu. Rev. Microbiol. **62:**93–111. http://dx.doi.org/10.1146/annurev.micro.62.081307.162737.
10. **Schwarz G, Mendel RR, Ribbe MW.** 2009. Molybdenum cofactors, enzymes and pathways. Nature **460:**839–847. http://dx.doi.org/10.1038/nature08302.
11. **Rubio LM, Singer SW, Ludden PW.** 2004. Purification and characterization of NafY (apodinitrogenase γ subunit) from *Azotobacter vinelandii*. J. Biol. Chem. **279:**19739–19746. http://dx.doi.org/10.1074/jbc.M400965200.
12. **Rubio LM, Rangaraj P, Homer MJ, Roberts GP, Ludden PW.** 2002. Cloning and mutational analysis of the gamma gene from *Azotobacter vinelandii* defines a new family of proteins capable of metallocluster-binding and protein stabilization. J. Biol. Chem. **277:**14299–14305. http://dx.doi.org/10.1074/jbc.M107289200.
13. **Seefeldt LC, Hoffman BM, Dean DR.** 2009. Mechanism of Mo-dependent nitrogenase. Annu. Rev. Biochem. **78:**701–722. http://dx.doi.org/10.1146/annurev.biochem.78.070907.103812.
14. **Dixon R, Kahn D.** 2004. Genetic regulation of biological nitrogen fixation. Nat. Rev. Microbiol. **2:**621–631. http://dx.doi.org/10.1038/nrmicro954.
15. **Martinez-Argudo I, Little R, Shearer N, Johnson P, Dixon R.** 2004. The NifL-NifA system: a multidomain transcriptional regulatory complex that integrates environmental signals. J. Bacteriol. **186:**601–610. http://dx.doi.org/10.1128/JB.186.3.601-610.2004.
16. **Dos Santos PC, Dean DR.** 2011. Co-ordination and fine-tuning of nitrogen fixation in *Azotobacter vinelandii*. Mol. Microbiol. **79:**1132–1135. http://dx.doi.org/10.1111/j.1365-2958.2011.07541.x.
17. **Jacobson MR, Brigle KE, Bennett LT, Setterquist RA, Wilson MS, Cash VL, Beynon J, Newton WE, Dean DR.** 1989. Physical and genetic map of

the major *nif* gene cluster from *Azotobacter vinelandii*. J. Bacteriol. **171:** 1017–1027.
18. **Jacobson MR, Cash VL, Weiss MC, Laird NF, Newton WE, Dean DR.** 1989. Biochemical and genetic analysis of the *nifUSVWZM* cluster from *Azotobacter vinelandii*. Mol. Gen. Genet. **219:**49–57.
19. **Hamilton TL, Jacobson M, Ludwig M, Boyd ES, Bryant DA, Dean DR, Peters JW.** 2011. Differential accumulation of *nif* structural gene mRNA in *Azotobacter vinelandii*. J. Bacteriol. **193:**4534–4536. http://dx.doi.org/10.1128/JB.05100-11.
20. **Temme K, Zhao D, Voigt CA.** 2012. Refactoring the nitrogen fixation gene cluster from *Klebsiella oxytoca*. Proc. Natl. Acad. Sci. U. S. A. **109:** 7085–7090. http://dx.doi.org/10.1073/pnas.1120788109.
21. **Curatti L, Ludden PW, Rubio LM.** 2006. NifB-dependent *in vitro* synthesis of the iron-molybdenum cofactor of nitrogenase. Proc. Natl. Acad. Sci. U. S. A. **103:**5297–5301. http://dx.doi.org/10.1073/pnas.0601115103.
22. **Robinson AC, Burgess BK, Dean DR.** 1986. Activity, reconstitution, and accumulation of nitrogenase components in *Azotobacter vinelandii* mutant strains containing defined deletions within the nitrogenase structural gene cluster. J. Bacteriol. **166:**180–186.
23. **Curatti L, Brown CS, Ludden PW, Rubio LM.** 2005. Genes required for rapid expression of nitrogenase activity in *Azotobacter vinelandii*. Proc. Natl. Acad. Sci. U. S. A. **102:**6291–6296. http://dx.doi.org/10.1073/pnas.0501216102.
24. **Shah VK, Davis LC, Brill WJ.** 1972. Nitrogenase. I. Repression and derepression of the iron-molybdenum and iron proteins of nitrogenase in *Azotobacter vinelandii*. Biochim. Biophys. Acta **256:**498–511.
25. **Sambrook J, Russell DW.** 2001. Molecular cloning: a laboratory manual, 3rd ed. Cold Spring Harbor Laboratory Press, Cold Spring Harbor, NY.
26. **Page WJ, von Tigerstrom M.** 1979. Optimal conditions for transformation of *A. vinelandii*. J. Bacteriol. **139:**1058–1061.
27. **Pfaffl MW.** 2004. Quantification strategies in real-time PCR, p 87–112. *In* Bustin SA (ed), A-Z of quantitative PCR. International University Line, La Jolla, CA.
28. **Barrios H, Valderrama B, Morett E.** 1999. Compilation and analysis of sigma(54)-dependent promoter sequences. Nucleic Acids Res. **27:**4305–4313. http://dx.doi.org/10.1093/nar/27.22.4305.
29. **Goosen N, van de Putte P.** 1995. The regulation of transcription initiation by integration host factor. Mol. Microbiol. **16:**1–7. http://dx.doi.org/10.1111/j.1365-2958.1995.tb02386.x.
30. **Crooks GE, Hon G, Chandonia JM, Brenner SE.** 2004. WebLogo: a sequence logo generator. Genome Res. **14:**1188–1190. http://dx.doi.org/10.1101/gr.849004.
31. **Smith PK, Krohn RI, Hermanson GT, Mallia AK, Gartner FH, Provenzano MD, Fujimoto EK, Goeke NM, Olson BJ, Klenk DC.** 1985. Measurement of protein using bicinchoninic acid. Anal. Biochem. **150:** 76–85. http://dx.doi.org/10.1016/0003-2697(85)90442-7.
32. **Laemmli UK.** 1970. Cleavage of structural proteins during the assembly of the head of bacteriophage T4. Nature **227:**680–685. http://dx.doi.org/10.1038/227680a0.
33. **Brandner JP, McEwan AG, Kaplan S, Donohue TJ.** 1989. Expression of the *Rhodobacter sphaeroides* cytochrome c2 structural gene. J. Bacteriol. **171:**360–368.
34. **Hernandez JA, Igarashi RY, Soboh B, Curatti L, Dean DR, Ludden PW, Rubio LM.** 2007. NifX and NifEN exchange NifB cofactor and the VK-cluster, a newly isolated intermediate of the iron-molybdenum cofactor biosynthetic pathway. Mol. Microbiol. **63:**177–192. http://dx.doi.org/10.1111/j.1365-2958.2006.05514.x.
35. **Shah VK, Brill WJ.** 1973. Nitrogenase. IV. Simple method of purification to homogeneity of nitrogenase components from *Azotobacter vinelandii*. Biochim. Biophys. Acta **305:**445–454.
36. **Hernandez JA, Curatti L, Aznar CP, Perova Z, Britt RD, Rubio LM.** 2008. Metal trafficking for nitrogen fixation: NifQ donates molybdenum to NifEN/NifH for the biosynthesis of the nitrogenase FeMo-cofactor. Proc. Natl. Acad. Sci. U. S. A. **105:**11679–11684. http://dx.doi.org/10.1073/pnas.0803576105.
37. **Stewart WPD, Fitzgerald GP, Burris RH.** 1967. *In situ* studies on N_2 fixation using the acetylene reduction technique. Proc. Natl. Acad. Sci. U. S. A. **58:**2071–2078. http://dx.doi.org/10.1073/pnas.58.5.2071.
38. **Martinez-Noel G, Curatti L, Hernandez JA, Rubio LM.** 2011. NifB and NifEN protein levels are regulated by ClpX2 under nitrogen fixation conditions in *Azotobacter vinelandii*. Mol. Microbiol. **79:**1182–1193. http://dx.doi.org/10.1111/j.1365-2958.2011.07540.x.
39. **Lee E-J, Groisman A.** 2010. An antisense RNA that governs the expression kinetics of a multifunctional virulence gene. Mol. Microbiol. **76:**1020–1033. http://dx.doi.org/10.1111/j.1365-2958.2010.07161.x.
40. **Kennedy C, Dean D.** 1992. The *nifU*, *nifS* and *nifV* gene products are required for activity of all three nitrogenases of *Azotobacter vinelandii*. Mol. Gen. Genet. **231:**494–498.
41. **Drummond M, Walmsley J, Kennedy C.** 1996. Expression from the *nifB* promoter of *Azotobacter vinelandii* can be activated by NifA, VnfA, or AnfA transcriptional activators. J. Bacteriol. **178:**788–792.
42. **Lei S, Pulakat L, Gavini N.** 1999. Regulated expression of the *nifM* of *Azotobacter vinelandii* in response to molybdenum and vanadium supplements in Burk's nitrogen-free growth medium. Biochem. Biophys. Res. Commun. **264:**186–190.
43. **Premakumar R, Pau RN, Mitchenall LA, Easo M, Bishop PE.** 1998. Regulation of the transcriptional activators AnfA and VnfA by metals and ammonium in *Azotobacter vinelandii*. FEMS Microbiol. Lett. **164:**63–68.
44. **Rodríguez-Quiñones F, Bosch R, Imperial J.** 1993. Expression of the *nifBfdxNnifOQ* region of *Azotobacter vinelandii* and its role in nitrogenase activity. J. Bacteriol. **175:**2926–2935.
45. **Hu Y, Fay AW, Lee CC, Ribbe MW.** 2007. P-cluster maturation on nitrogenase MoFe protein. Proc. Natl. Acad. Sci. U. S. A. **104:**10424–10429. http://dx.doi.org/10.1073/pnas.0704297104.
46. **Robinson AC, Dean DR, Burgess BK.** 1987. Iron-molybdenum cofactor biosynthesis in *Azotobacter vinelandii* requires the iron protein of nitrogenase. J. Biol. Chem. **262:**14327–14332.
47. **Kim CH, Newton WE, Dean DR.** 1995. Role of the MoFe protein alpha-subunit histidine-195 residue in FeMo-cofactor binding and nitrogenase catalysis. Biochemistry **34:**2798–2808.
48. **Hernandez JA, Phillips AH, Erbil WK, Zhao D, Demuez M, Zeymer C, Pelton JG, Wemmer DE, Rubio LM.** 2011. A sterile α-motif domain in NafY targets apo-NifDK for iron-molybdenum cofactor delivery via a tethered domain. J. Biol. Chem. **286:**6321–6328. http://dx.doi.org/10.1074/jbc.M110.168732.
49. **Hill S.** 1992. Physiology of nitrogen fixation in free-living heterotrophs, p 87–134. *In* Stacey G, Burris RH, Evans HJ (ed), Biological nitrogen fixation. Chapman-Hall, New York, NY.
50. **Gorini L, Maas WK.** 1957. The potential for the formation of a biosynthetic enzyme in *Escherichia coli*. Biochim. Biophys. Acta **25:**208–209.